

Magnetic ground state and Fermi surface of bcc Eu

J. Kuneš

Department of Physics, University of California, One Shields Avenue, Davis, California 95616, USA and Institute of Physics, Academy of Sciences of the Czech Republic, Cukrovarnická 10, 162 53 Praha 6, Czech Republic

R. Laskowski

Institut for Fysik og Astronomi Aarhus Universitet, Ny Munkegade, 8000 Aarhus C, Denmark

(Received 8 April 2004; revised manuscript received 25 August 2004; published 12 November 2004)

Using spin-spiral technique within the full potential linearized augmented-plane-waves (LAPW) electronic structure method, we investigate the magnon spectrum and Néel temperature of bcc Eu. Ground state corresponding to an incommensurate spin spiral is obtained in agreement with experiment and previous calculations. We demonstrate that the magnetic coupling is primarily through the intra-atomic f - s and f - d exchange and Ruderman-Kittel-Kasuya-Yosida mechanism. We show that the existence of this spin spiral is closely connected to a nesting feature of the Fermi surface, which was not noticed before.

DOI: 10.1103/PhysRevB.70.174415

PACS number(s): 75.10.Hk, 71.18.+y, 71.27.+a

I. INTRODUCTION

The magnetic behavior of most rare-earth (RE) materials is governed by localized magnetic moments interacting indirectly through the sea of delocalized valence electrons. A typical feature of RE systems is existence of two electron species, localized $4f$'s exhibiting atomiclike behavior with strong Coulomb interaction and delocalized $5d$ and $6s$ electrons with interaction merely renormalizing the band dispersion. Yet, a typically weak interaction between these two species, either due to intra-atomic exchange or band mixing (hybridization), gives rise to a variety of magnetic behaviors.¹ On the model level this behavior is captured by the periodic Anderson model or Kondo lattice model.² The *ab initio* electronic structure methods based on density functional theory (DFT)³ and the standard semi-local approximations^{4,5} have notorious problems in dealing with the strong correlations within the $4f$ shell. In particular, the splitting between occupied and unoccupied $4f$ bands, which is the way a single-particle band structure can capture the effect of Coulomb interaction, is missing. Consequently, the f bands appear at the Fermi level, resulting in unrealistic filling of both f and valence orbitals. Two remedies can be used: (i) open-core treatment or (ii) additional Coulomb term with the simplest example being the LDA+U method. In the open-core treatment the $4f$ orbitals are kept separate from the rest of the valence Hamiltonian, and the interaction with the valence states is only through the self-consistent potential. Obviously, the proper filling of both f and valence bands is easy to achieve if integer, however, all kinematic exchange effects (e.g., superexchange) based on band mixing are missing. In the LDA+U approach, the splitting between the occupied and unoccupied f band is obtained due to an additional orbital-dependent term. All possible exchange processes are, in principle, accounted for in this approach.

Compounds containing Eu in 2+ formal valency are particularly well suited for LDA+U treatment, because the orbital degrees of freedom are quenched in the half filled f shell. Examples involve ferromagnetic insulators EuO and EuS,⁶ semimetal EuB₆ (Ref. 7) and metallic elemental Eu.

Presumably the exchange mechanisms in these materials are quite different.

In this paper we investigate the magnetic ground state and magnon spectrum of elemental Eu. Europium crystallizes in body-centered cubic (bcc) structure with a lattice constant⁸ of 4.555 Å at 100 K. The magnetic groundstate was found to be a spin spiral and the Néel temperature^{8,9} of 91 K. The electronic structure was previously investigated by Freeman and Dimmock¹⁰ and Andersen and Loucks¹¹ using the $X\alpha$ potential. Recently, Turek *et al.*¹² used a real-space perturbation approach based on tight-binding linear muffin-tin orbital (TB-LMTO) method to calculate the exchange parameters and corresponding magnon spectrum and Néel temperature. Here we use a reciprocal space based spin spiral approach which can be viewed as complementary to the real space calculations. Unlike the above authors who used the open core treatment of the $4f$ orbitals we employ the LDA+U method. We use the linearized augmented-plane-waves (LAPW)¹³ method and its extension to non-collinear magnetic structures utilizing the generalized Bloch theorem¹⁴ for calculation of the spin spiral states. We interpret our results in terms of Ruderman-Kittel-Kasuya-Yosida (RKKY) exchange mechanism¹⁵⁻¹⁷ and the Fermi surface property. For this purpose we evaluate the low frequency limit of the generalized susceptibility and identify the nesting features of the Fermi surface.

II. COMPUTATIONAL METHOD

We have used the Wien2k¹⁸ implementation of the full potential LAPW method and its extension for noncollinear spin structures.¹⁹ The effective single-particle potential was constructed from the LDA+U functional, with the exchange-correlation potential of Perdew and Wang⁵ and the double-counting scheme of Anisimov *et al.*²⁰ The Coulomb term parametrized with U (7 eV unless stated otherwise), and J (0.75 eV) was applied to the $4f$ orbitals. The spin spirals were treated using the generalized Bloch theorem,¹⁴ which prohibits inclusion of the spin-orbit coupling. The atomic

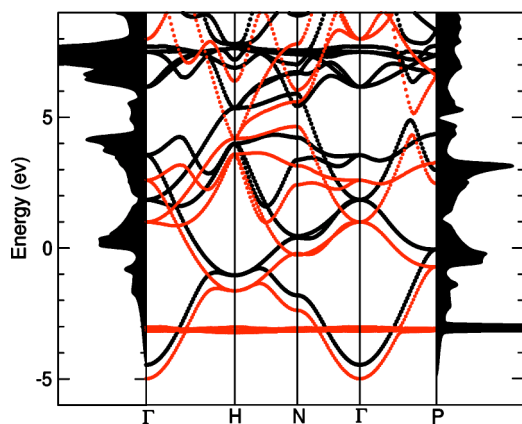


FIG. 1. (Color online) The band structure as obtained with LDA+U method. The brighter (red) lines correspond to majority spin. In the side panels the corresponding densities of state for the minority (left) and majority (right) spin projections are shown.

sphere approximation was employed, in which the direction of the exchange field is constrained inside atomic spheres and allowed to vary continuously in the interstitial space.

A spin spiral is defined by a propagation vector \mathbf{q} and angle θ between the local moment and the precession axis. The orientation of the precession axis itself is arbitrary unless the spin-orbit coupling is taken into account. Each spin spiral was calculated self-consistently. This approach has two deficiencies compared to the perturbative approach employing the force theorem:²¹ (i) it takes much more computational effort, (ii) more importantly, one has to work with total energies instead of the sums of eigenvalues (i.e., looking at small differences of large numbers, which requires high accuracy). As for (i), when performing calculations for \mathbf{q} -vectors along a certain path in the reciprocal space, converged spin density from a nearby \mathbf{q} can be used as the starting point, which reduces the number of iteration needs significantly compared to starting from scratch for each \mathbf{q} . As for (ii), θ dependence of spin-spiral energies can be studied without being limited to small angles.

III. RESULTS AND DISCUSSION

A. Bandstructure

In Fig. 1 we show the spin-projected band structure obtained with U of 7 eV and J of 0.75 eV. The lowest valence band around the Γ point with a predominant 6s character corresponds to a strongly dispersive s band. Moving toward the zone boundary mixing with the d band takes place and the doublets at H and P points have a pure d symmetry. The states in the vicinity of the Fermi level have mostly d character.

The occupied 4f levels are localized about 3 eV below the Fermi level and cross the lowest valence band, with negligible hybridization, which is reflected by completely flat dispersion. The unoccupied 4f bands are approximately 7 eV above the Fermi level. A bandwidth of about 2 eV originates from mixing with the 6p and 5d bands. Lack of mixing with valence states in the occupied f bands indicates that the ki-

nematic exchange, involving hopping from localized f orbitals into the delocalized band states, is not important here. The interaction between the localized f states and the rest of the electronic system is dominated by intra-atomic f-s and f-d exchange. Consequently, the spin polarized bands and density of states below 2 eV exhibit almost a perfect rigid shift. The deviations from this pattern are due to the difference between the f-d and f-s intra-atomic exchange.

B. Magnon spectrum

The magnetic excitations are discussed in terms of a classical Heisenberg Hamiltonian

$$H = - \sum_{\mathbf{R}\mathbf{R}'} J_{\mathbf{R}\mathbf{R}'} \mathbf{e}_{\mathbf{R}} \cdot \mathbf{e}_{\mathbf{R}'}. \quad (1)$$

A spin spiral characterized by the propagation vector \mathbf{q} and angle θ has the form

$$\mathbf{e}_{\mathbf{R}} = [\sin(\theta)\cos(\mathbf{q} \cdot \mathbf{R}), \sin(\theta)\sin(\mathbf{q} \cdot \mathbf{R}), \cos(\theta)]. \quad (2)$$

The corresponding energy per lattice site obtained from (1)

$$E(\mathbf{q}) = \sin^2(\theta)[J(\mathbf{q}) - J(0)] + J(0) + E_0 \quad (3)$$

$$J(\mathbf{q}) = \sum_{\mathbf{R}} J_{0\mathbf{R}} \exp(i\mathbf{q} \cdot \mathbf{R}) \quad (4)$$

is to be compared to the *ab initio* results. E_0 is the nonmagnetic part of the total energy. Note that only the difference $J(\mathbf{q}) - J(0)$ can be obtained from the knowledge of $E(\mathbf{q})$. In order to fix the value of $J(\mathbf{q})$ the sum rule

$$\int d\mathbf{q} J(\mathbf{q}) = 0, \quad (5)$$

where the integration is over the Brillouin zone, is to be employed. The $J(\mathbf{q})$ normalized this way contains only information about the intersite $J_{\mathbf{R}\mathbf{R}'}$ and can be related to the ordering temperature, which is discussed below.

Using the Hamiltonian (1) involves several approximations. Quenching of the orbital moment in a half filled shell, rigidity of the f moment and its size ($S=7/2$) well justify the use of Heisenberg Hamiltonian in classical approximation. In addition we assume that the exchange parameters are constant. This is not *a priori* guaranteed, since the electronic structure of the band electrons, which carry the exchange interaction between the local f moments, depends on the arrangement of local moments. This question was discussed in detail by Nolting *et al.*²² who derived an expression for the effective exchange parameters $J_{\mathbf{R}\mathbf{R}'}$ in terms of the conduction electron self-energy. Experimentally this leads to temperature dependence of the effective exchange parameters. If this effect were important, then a deviation from the θ dependence of Eq. (3) would have been expected. The fact that we have not found any significant deviation from (3) in the range from 90° to 30° serves as a justification of use of Hamiltonian (1). This is also in agreement with a rather big ratio of the bandwidth to the exchange splitting in the conduction band.

In Fig. 2 we show the \mathbf{q} -dependent exchange parameter obtained with maximum θ of 90°. Calculations performed

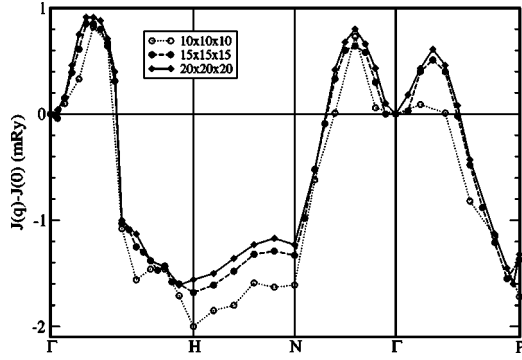


FIG. 2. The \mathbf{q} -dependent exchange parameter calculated using the spin-spiral approach. Comparison of the results for different k -point samplings indicates that the $15 \times 15 \times 15$ mesh is reasonably well converged.

with U of 6 eV and 8 eV lead to almost identical dispersion supporting our previous conclusion about the f - d exchange mechanism, which does not depend on the position of the f bands. The calculations yield a minimum energy corresponding to a spiral with propagation vector \mathbf{Q} of $(0.27 \pm 0.01) \times (2\pi/a, 0, 0)$ and another two local minima along ΓN and ΓP lines. The ground-state spin spiral corresponds to the rotation of the magnetization vector by $(49 \pm 2)^\circ$, which value corresponds very well to both theoretical¹² and experimental^{8,9} results.

In order to address the Néel temperature, the $E(\mathbf{q})$ throughout the Brillouin zone is needed. To this end we have calculated the spin spirals on a $10 \times 10 \times 10$ regular \mathbf{q} grid (44 irreducible \mathbf{q} points) and used a smooth Fourier interpolation²³⁻²⁵ to obtain $J(\mathbf{q})$ on a denser grid. In Fig. 3 we compare the interpolating function to the *ab initio* results along the high symmetry directions. Since only a few high symmetry \mathbf{q} -points were contained in the regular grid, the agreement between the interpolating function and the *ab initio* data points indicates the quality of the grid. Comparison to the results obtained by Turek *et al.* reveals a very good agreement of the key features. In order to facilitate a detailed

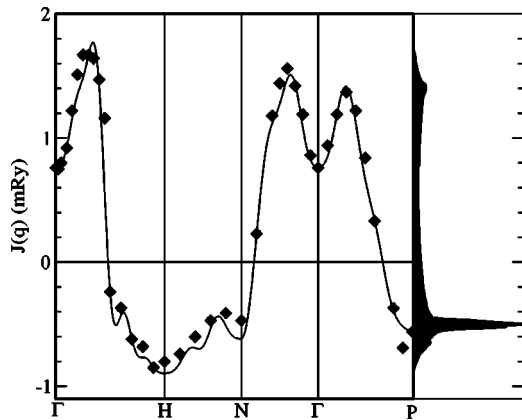


FIG. 3. The \mathbf{q} -dependent exchange parameter renormalized to satisfy the sum rule (5) along the high symmetry lines; *ab initio* data (symbols), Fourier interpolation (line). The right panel shows the corresponding density of states.

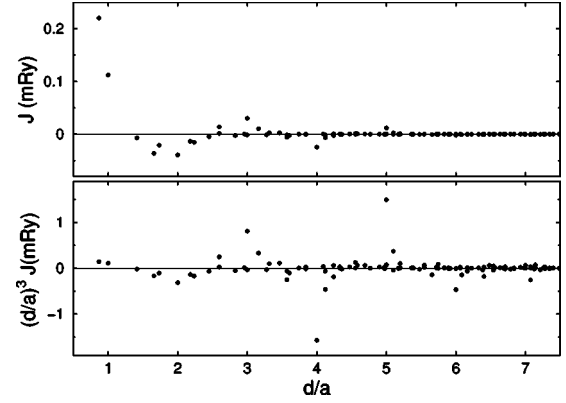


FIG. 4. The exchange parameter as a function of the interatomic distance (upper panel). The same curve with the d^3 prefactor (bottom panel) reveals the RKKY oscillations.

comparison of the real space and reciprocal space approaches we present in Fig. 4 the exchange parameters as a function of the real space distance obtained by the Fourier interpolation. Besides the similar overall shape of the spectrum, we have obtained the same ordering of the peak according to their size as well as similar absolute values. The most apparent deviation is the position of the ferromagnetic state $J(0)$, which is relatively more favorable in our calculation. Evaluating the expressions¹² for Néel temperature in the mean-field (T_N^{MF}) and random-phase (T_N^{RPA}) approximations

$$k_B T_N^{MF} = \frac{2}{3} J(\mathbf{Q}) \quad (6)$$

$$(k_B T_N^{RPA})^{-1} = \frac{3}{4N} \sum_{\mathbf{q}} \left\{ [J(\mathbf{Q}) - J(\mathbf{q})]^{-1} + \left[J(\mathbf{Q}) - \frac{1}{2} J(\mathbf{q} + \mathbf{Q}) - \frac{1}{2} J(\mathbf{q} - \mathbf{Q}) \right]^{-1} \right\} \quad (7)$$

with the interpolating function we arrive at $T_N^{MF} = 170$ K and $T_N^{RPA} = 112$ K which again agree very well with 147 K and 110 K obtained by Turek *et al.* as well as with the experimental value^{8,9} of 90.5 K.

C. Fermi surface and nesting

In this section we discuss the paramagnetic Fermi surface and its connection to the spin-spiral ground state. Very fine k -point sampling is required in order to study the fine details of the Fermi surface. We adopted the following approach. Starting with 100 irreducible k -points obtained with LAPW code we have used the procedure for smooth Fourier interpolation²³⁻²⁵ for the bands at the Fermi energy. We have generated the band energies on a finer mesh of approximately 1.5×10^6 k -points in the whole Brillouin zone, which was used for the calculations reported below. In Fig. 5 we show the paramagnetic band structure together with the Fourier interpolation, which is excellent near E_F (note that the interpolation was performed on different regular mesh).

The paramagnetic Fermi surface of bcc Eu (Fig. 6) consists of an electron pocket centered at H point, and a hole

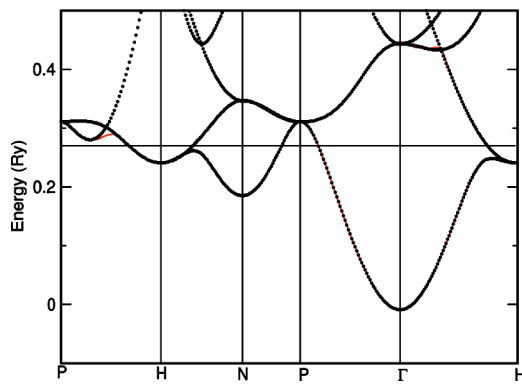


FIG. 5. (Color online) The paramagnetic *ab initio* bands (dots) together with the smooth Fourier interpolation of the low valence bands (red lines). Note that the inaccuracies of the fit at the band crossings (for example midway between P and H) are far from the Fermi level.

pocket located at P point. Symmetry related degeneracy of the valence band along the P-H direction results in touching of these pockets. The first numerical investigation of the Fermi surface of bcc Eu was reported by Andersen and Loucks,¹¹ who called these pockets “superegg” and “tetrahedron,” respectively. While our calculation reproduces the superegg shape, contrary to Andersen’s cube with lobes we find rather a rounded tetrahedron with lobes.

In order to make connection between the Fermi surface geometry and calculated spin-spiral dispersion, we have evaluated the imaginary part of the generalized susceptibility

$$\chi_{ij}(\mathbf{q}, \omega) = - \sum_{\mathbf{k}} \frac{f(\epsilon_i(\mathbf{k})) - f[\epsilon_j(\mathbf{k} + \mathbf{q})]}{\epsilon_i(\mathbf{k}) - \epsilon_j(\mathbf{k} + \mathbf{q}) - \omega + i0^+}, \quad (8)$$

where $\epsilon(\mathbf{k})$ is the band energy, $f(\epsilon)$ is the Fermi-Dirac function, and i and j are band indices. In the limit $\omega \rightarrow 0$, the imaginary part of $\chi(\mathbf{q}, \omega)$ behaves as

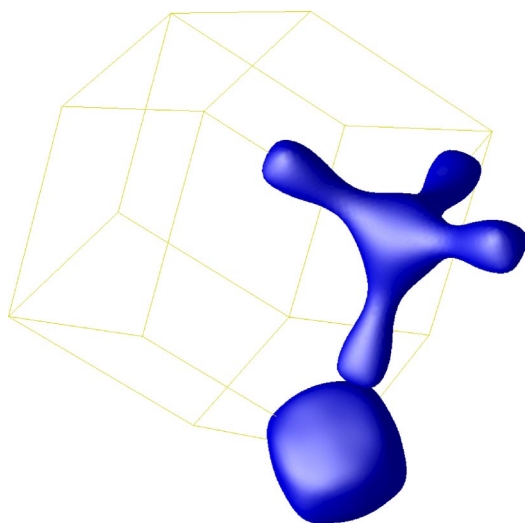


FIG. 6. The paramagnetic Fermi surface. The lobed tetrahedra are centered at 8 P points and “supereggs” at 6 H points on the surface of the 1st Brillouin zone (only one representative of both species is shown for sake of clarity).

$$\text{Im } \chi_{ij}(\mathbf{q}, \omega) = \pi \omega \sum_{\mathbf{k}} \delta(\epsilon_i(\mathbf{k}) - \epsilon_F) \delta(\epsilon_j(\mathbf{k} + \mathbf{q}) - \epsilon_F) \quad (9)$$

$$= \pi \omega \nu_{ij}(\mathbf{q}), \quad (10)$$

where $\nu(\mathbf{q})$ measures so called nesting, i.e., the extent to which different parts of the Fermi surface weighted by the inverse square of the Fermi velocity are parallel. While the real part of the generalized susceptibility is directly related to the exchange parameters $J(\mathbf{q})$, it is the imaginary part that has a straightforward geometrical interpretation. The real and imaginary parts are bound by the Kramers-Kronig relations, which, for the $\omega=0$ limit, read

$$\text{Re } \chi(\mathbf{q}, \omega = 0) = \frac{1}{\pi} \int_{-\infty}^{+\infty} d\omega' \frac{\text{Im } \chi(\mathbf{q}, \omega')}{\omega'}. \quad (11)$$

Comparing this to (9), one can readily see that a peak in $\nu(\mathbf{q})$ provides a significant contribution to a peak in $\text{Re } \chi(\mathbf{q}, \omega = 0)$. In the special case $\mathbf{q} \rightarrow 0$ limit, $\nu(\mathbf{q})$ diverges as $1/|q|$,

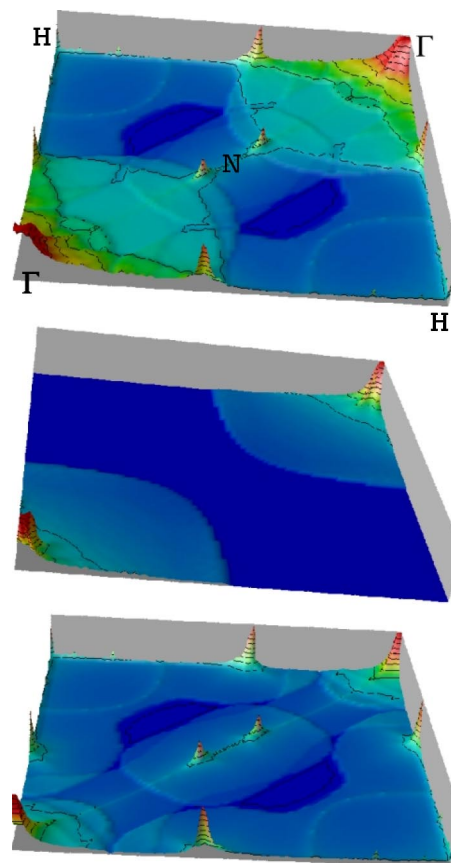


FIG. 7. (Color online) The nesting function in the Γ HNH plane. The lower-left and upper-right corners correspond to the Γ point with the typical $1/q$ divergence; the remaining corners are at the H point, and the N point is in the center of the square. The upper panel shows the sum over all (2) bands. The middle panel shows the “superegg” contribution and the lower panel the lobed tetrahedra contribution (the contribution of the superegg-to-lobed tetrahedron processes is not shown).

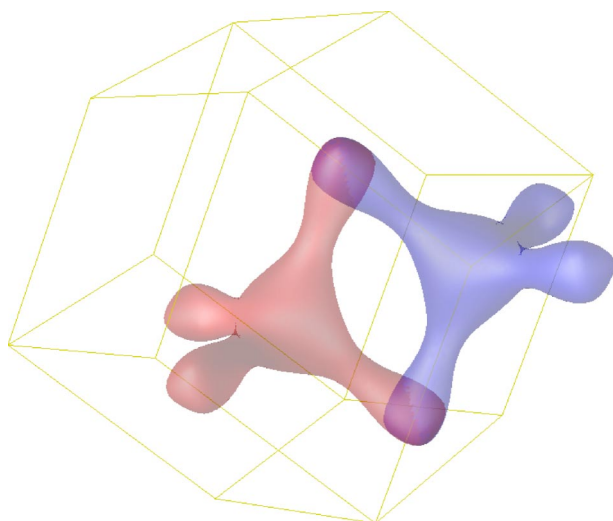


FIG. 8. The lobed tetrahedron translated by $\mathbf{q}=0.4 \times (2\pi/a, 0, 0)$ corresponding to the Γ -H peak elucidates the origin of the spin-spiral ground state.

however, the limit $\lim_{q \rightarrow 0} \lim_{\omega \rightarrow 0} \text{Re } \chi(\mathbf{q}, \omega)$ remains finite, equal to the density of states (or corresponding partial density of states) at the Fermi level $N(\epsilon_F)$. In general, peaks in $\nu(\mathbf{q})$ indicate a tendency toward instability of the Fermi surface toward formation of incommensurate structures, such as spin- or charge-density waves.

Andersen and Loucks concluded that the origin of the spin-spiral ground state is the nesting between the opposite faces of their “tetracube.” However, our investigation provides a different picture. In Fig. 7 we show the nesting function $\nu(\mathbf{q})$ in the Γ HNH plane. There is a prominent peak on the Γ -H line and a weaker feature on the Γ -N line. In order to identify the origin of these features, we have calculated, separately, the contributions of the different sheets of the Fermi surface. Figure 7 demonstrates that both peaks originate from transitions between the lobed tetrahedra surfaces. The \mathbf{q} parallel to the Γ -H direction amounts to moving the lobed tetrahedron centered at the P point toward the next P point on the same face. The peak on the Γ -H line corresponds to the overlap of the lobes, which is illustrated explicitly in Fig. 8. The peak on the Γ -N line corresponds to the sum of two nesting vectors along adjacent Γ -H directions. Therefore, it originates from an overlap of the tips of the lobes, however, belonging to tetrahedra centered at P points, which are not on the same face. In Fig. 9 we show the nesting function in the Γ HPN plane. Besides the peaks on Γ -H and Γ -N lines, we find weaker features on the Γ -P line. Analysis of the contributions from different sheets shows that these features originate from transitions between the two types of Fermi surfaces.

Eventually we can compare the information obtained from the nesting function to the magnon dispersion. We have found a prominent nesting feature on the Γ -H line and weaker one on the Γ -N line. These are related to the minima in the spin-spiral energies. The energy minima do not sit exactly at the positions of corresponding the nesting vectors. While the nesting vectors contain information about the

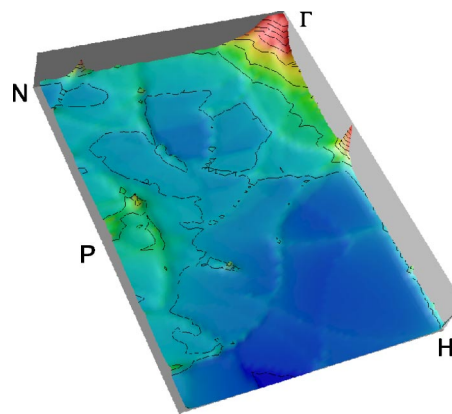


FIG. 9. (Color online) The nesting function in the Γ HPN plane. The arc-shaped features intersecting the Γ P line originate from superegg-to-lobed tetrahedron processes.

states directly at the Fermi energy, all states contribute to the spin-spiral minima, yet with a weight decreasing with the distance from the Fermi level. A discussion of the generalized susceptibility in the context of electron-phonon coupling can be found in Ref. 26. The features on the Γ -P line are rather weak and do not fit well with the position of the Γ -P peak; therefore, we do not draw any conclusion about its direct relation to the local energy minimum on the Γ -P line.

IV. CONCLUSIONS

Using a full-potential method with the LDA+U functional and spin-spiral approach, we have obtained a magnon spectrum that is in good agreement with that of Turek *et al.*¹² using TB-LMTO. The calculations reproduce well the experimentally observed spin-spiral ground state and provide a reasonable estimate of the Néel temperature. The good agreement of two rather different computational methods indicates a robustness of these physical properties. Moreover, we have shown that the values of the exchange parameters are insensitive to the precession angle of the spin spiral as well as the value of U, i.e., exact position of the occupied f bands. This confirms the picture of bcc Eu as a Kondo-lattice system with ferromagnetic exchange of intra-atomic origin in the RKKY regime. We have identified the origin of the spin-spiral ground state in terms of nesting properties of the Fermi surface. In particular we have shown that the nesting is connected to the lobed tetrahedron hole pockets centered at the P point of the Brillouin zone.

ACKNOWLEDGMENTS

We wish to acknowledge the helpful discussions and numerous suggestions by W. E. Pickett, J. Kudrnovský, and P. Novák. This work was supported by Department of Energy Grant No. DE-FG 03-01ER45876, Grant No. A1010214 from Academy of Sciences of the Czech Republic, and by the Czech-USA project KONTAKT ME547.

- ¹J. Jensen and A. R. Mackintosh, *Rare Earth Magnetism* (Clarendon, Oxford, 1991).
- ²A. C. Hewson, *Kondo Problem to Heavy Fermions* (Cambridge University Press, Cambridge, England, 1993).
- ³P. Hohenberg and W. Kohn, Phys. Rev. **136**, B864 (1964).
- ⁴W. Kohn and L. Sham, Phys. Rev. **140**, A1133 (1965).
- ⁵J. P. Perdew and Y. Wang, Phys. Rev. B **45**, 13244 (1992).
- ⁶P. Wachter, *Handbook of Physics and Chemistry of Rare Earth*, Vol. 1 (North-Holland, Amsterdam, 1979).
- ⁷The question whether stoichiometric EuB_6 is actually semimetal or semiconductor is still controversial.
- ⁸N. G. Nereson, C. E. Olsen, and G. P. Arnold, Phys. Rev. **135** A176 (1964).
- ⁹A. H. Millhouse and K. A. McEwen, Solid State Commun. **13**, 339 (1973).
- ¹⁰A. J. Freeman and J. O. Dimmock, Bull. Am. Phys. Soc. **11**, 216 (1966).
- ¹¹O. K. Andersen and T. L. Loucks, Phys. Rev. **167**, 551 (1968).
- ¹²I. Turek, J. Kudrnovský, M. Diviš, P. Franek, G. Bihlmayer, and S. Blügel, Phys. Rev. B **68**, 224431 (2003).
- ¹³D. J. Singh, *Plane Waves, Pseudopotentials and the LAPW Method* (Kluwer, Boston, 1994).
- ¹⁴L. M. Sandratskii, Adv. Phys. **47**, 91 (1998).
- ¹⁵M. A. Rudeman and C. Kittel, Phys. Rev. **96**, 99 (1954).
- ¹⁶K. Yosida, Phys. Rev. **106**, 893 (1957).
- ¹⁷T. Kasuya, Prog. Theor. Phys. **16**, 45 (1956).
- ¹⁸P. Blaha, K. Schwarz, G. K. H. Madsen, D. Kvasnicka, and J. Luitz, *WIEN2k, An Augmented Plane Wave+Local Orbitals Program for Calculating Crystal Properties* (Karlheinz Schwarz, Techn. Universität Wien, Wien, 2001).
- ¹⁹R. Laskowski, G. K. H. Madsen, P. Blaha, and K. Schwarz, Phys. Rev. B **69**, 140408 (2004).
- ²⁰V. I. Anisimov, I. V. Solovyev, M. A. Korotin, M. T. Czyzyk, and G. A. Sawatzky, Phys. Rev. B **48**, 16929 (1993).
- ²¹A. I. Lichtenstein, M. I. Katsnelson, V. P. Andropov, and V. A. Gubanov, J. Magn. Magn. Mater. **67**, 65 (1987).
- ²²W. Nolting, S. Rex, and S. M. Jaya, J. Phys.: Condens. Matter **9**, 1301 (1997).
- ²³W. E. Pickett, H. Krakauer, and P. B. Allen, Phys. Rev. B **38**, 2721 (1988).
- ²⁴D. G. Shankland, *Computational Methods in Band Theory* (Plenum, New York, 1971), p. 362.
- ²⁵D. D. Koelling and J. H. Wood, J. Comput. Phys. **67**, 253 (1986).
- ²⁶S. K. Sinha and B. N. Harmon, Phys. Rev. Lett. **35**, 1515 (1975).